

Negative Feedback Training: A Novel Concept to Improve Robustness of NVCIM DNN Accelerators

Yifan Qin
University of Notre Dame
Notre Dame, IN, USA
yqin3@nd.edu

Zheyu Yan
University of Notre Dame
Notre Dame, IN, USA
zyan2@nd.edu

Wujie Wen
North Carolina State University
Raleigh, NC, USA
wwen2@ncsu.edu

Xiaobo Sharon Hu
University of Notre Dame
Notre Dame, IN, USA
shu@nd.edu

Yiyu Shi
University of Notre Dame
Notre Dame, IN, USA
yshi4@nd.edu

ABSTRACT

Compute-in-memory (CIM) accelerators built upon non-volatile memory (NVM) devices excel in energy efficiency and latency when performing Deep Neural Network (DNN) inference, thanks to their in-situ data processing capability. However, the stochastic nature and intrinsic variations of NVM devices often result in performance degradation in DNN inference. Introducing these non-ideal device behaviors during DNN training enhances robustness, but drawbacks include limited accuracy improvement, reduced prediction confidence, and convergence issues. This arises from a mismatch between the deterministic training and non-deterministic device variations, as such training, though considering variations, relies solely on the model’s final output. In this work, we draw inspiration from the control theory and propose a novel training concept: Negative Feedback Training (NFT) leveraging the multi-scale noisy information captured from network. We develop two specific NFT instances, Oriented Variational Forward (OVF) and Intermediate Representation Snapshot (IRS). Extensive experiments show that our methods outperform existing state-of-the-art methods with up to a 46.71% improvement in inference accuracy while reducing epistemic uncertainty, boosting output confidence, and improving convergence probability. Their effectiveness highlights the generality and practicality of our NFT concept in enhancing DNN robustness against device variations.

1 INTRODUCTION

Deep Neural Networks (DNNs) have ushered in a profound transformation in our society. However, accelerating DNN inference, which involves substantial vector-matrix computational loads, is hindered by frequent data movement between memory and processing units. This von Neumann bottleneck [2] could be solved by Computing-In-Memory (CIM) DNN accelerators [15]. Leveraging emerging Non-Volatile Memory (NVM) devices, NVCIM DNN accelerators perform parallel in-situ data processing, significantly outperforming their CMOS-based counterparts in terms of energy efficiency and density [22]. However, the inherent non-idealities of NVM devices, such as device variation, contribute to the deviation in device conductance values [1, 12, 13]. As a result, such deviations affect the represented model weights after programming and, consequently, have a detrimental impact on the inference accuracy of NVCIM DNN accelerators [18].

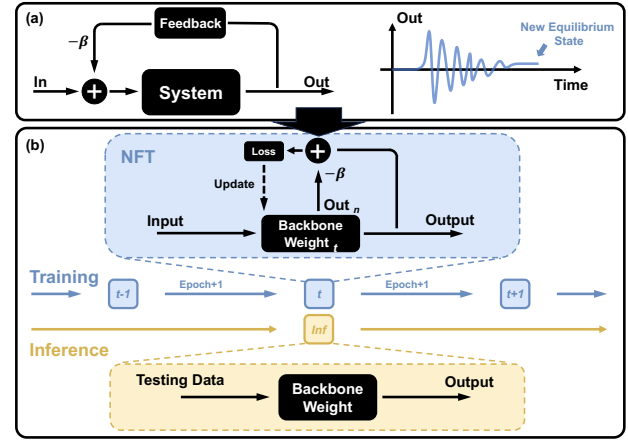


Figure 1: (a) Schematic diagram of a classic negative feedback system and the process of the system setting to a new equilibrium state. (b) Illustration of negative feedback training.

Achieving reliable DNN inference with unreliable NVM substrates is challenging. There exists a variety of hardware and software solutions to address this, such as device upgrade [3], write-verify [16], training regularization [4], neural architecture search [10, 18], and Bayesian network [6]. Among them, noise-injection (or noise-aware) training [9, 21] has emerged as one of the most popular and effective methods with no need for accelerator hardware modification. Simply exposing DNNs to the Gaussian noise (for modeling device variation) [11, 17, 19] at the training stage, it enhances the model’s noise tolerance. However, state-of-the-art (SOTA) noise-injection training methods are subject to issues like limited accuracy improvement, less confident prediction (or increased epistemic uncertainty [7]), and hard-to-reach training convergence under large variations. Our observation is that this mainly stems from the mismatch between the non-deterministic noise and the deterministic training for the following reasons: **First**, only a limited number of noise samples are exposed to the network during limited training epochs, hindering the network from fully capturing the pattern of noise behavior. **Second**, compared with vanilla training, the random noise samples in noise-injection training offer more diverse optimization directions to the network, but some may lead to incorrect states, and the associated uncertainty exacerbates this

trend. Therefore, the network may fail in converging to the optimal state during training, or the well-trained model may not generate high-quality predictions when confronted with variations in weight during inference.

We hypothesize that this mismatch can be alleviated by learning sufficient variation information from different points during the training process, rather than relying solely on the model’s final output, as adopted by SOTA methods. This conjecture is grounded in modern control theory, where stability relies on negative feedback. When a balanced system is perturbed by noise, negative feedback helps the system resist the perturbation and eventually reaches a new equilibrium state. Figure 1(a) shows a schematic diagram of this process. The feedback is generated from a portion of the outputs and controlled by the negative feedback coefficient β . Drawing inspiration from that, we introduce the concept of “**Negative Feedback Training (NFT)**” to DNNs. This innovative approach, involving negative contributions from different parts of the network’s outputs, mitigates the influence of noise and helps the neural network reach a more robust state, as depicted in Figure 1(b). At a high level, the **entire NFT process** can be described as follows: We employ NFT to enhance the robustness of the DNN backbone during the training process. Once the training is completed, all negative feedback components are removed, leaving only a pure and structurally unmodified, robust DNN backbone model. During training, negative feedback Out_n are generated from NFT and contribute negatively to the objective in weight update with coefficient β , improving DNN performance. The “negative” diminishes the bad impact of target variation while maintaining its subject status, and the “feedback” introduces additional noise information that is different from what the output of backbone contains to the objective. Together, “negative feedback” constrains network optimization based on the influence of noise itself, with stronger constraints corresponding to greater perturbations. This ensures that the network does not deviate too far from the optimal direction, facilitating stable convergence to the optimal state during training.

Our main contributions are as follows:

- We introduce a negative feedback mechanism into the DNN training process to stabilize it and enhance the DNN robustness to device variations. *To the best of our knowledge, this is the first of its kind.*
- We propose two novel implementations of the negative feedback training (NFT) concept: *Oriented Variational Forward (OVF)* and *Intermediate Representation Snapshot (IRS)*. Specifically, OVF optimizes the network from an overall variational performance perspective and IRS uses internal feature representations to constrain the training process.
- Our extensive simulations on NVCIM DNN accelerators with varying device variations demonstrate NFT’s effectiveness in mitigating sensitivity and output fluctuations, enhancing confidence and convergence probability while reducing epistemic uncertainty. For example, it achieves up to 46.71% improvement in DNN average inference performance compared to SOTA methods.

We believe our work represents an important step in reducing the mismatch between deterministic training and non-deterministic

device variations in DNN models for CIM accelerators, underscoring NFT’s potential as a new direction for improving DNN robustness.

2 BACKGROUND AND RELATED WORK

NVM device non-ideal factors. NVM devices are susceptible to various sources of variations and noise, encompassing spatial and temporal variations. Spatial variations stem from defects that arise during fabrication, while temporal variations result from stochastic fluctuations in the device material. Unlike spatial variations, temporal variations are usually independent of the device but are subject to the programmed value [5]. For example, temporal variations can lead to different conductance values for the same NVM device when identical programming pulses are applied. In our research, we consider non-idealities to be uncorrelated among NVM devices, but our method can be adapted to account for other distributions of variations with appropriate modifications.

Prior Work. To address the DNN performance degradation due to above NVM device variations, two main research directions exist: reducing device conductance variation (hardware) and improving DNN robustness in the presence of device variation (software). For example, device improvements can be achieved through advancements in material development and fabrication processes [3], and write-verify [16] operations can be applied during device programming. Recent research indicates that selectively write-verifying only critical devices can improve the accuracy [20]. Additionally, new circuits have been proposed to address device variations. On the software front, CorrectNet [4], which employs modified Lipschitz constant regularization during DNN training, is designed for robust DNNs. Other software-based methods involving training model weights with noises, designing architectures, and pruning techniques [6, 10, 18] are also proposed. In this work, we focus on noise-injection training—one of the most important software-based solutions to this problem.

3 PROPOSED METHOD

In this section, we introduce NFT and provide two implementation instances, *i.e.*, OVF and IRS, from different optimization angles.

3.1 Negative Feedback Training

Our proposed method draws on the negative feedback theory, a fundamental principle in system control. According to this theory, a system, when subjected to perturbation or disturbance, uses negative feedback to suppress or attenuate the perturbation, ultimately reaching a new equilibrium state. In our approach, we consider weight variations as a type of perturbation affecting the system. We aim to enhance the system robustness by suppressing such “noise” through negative feedback. The overall structure of NFT consists of a backbone DNN architecture and a negative feedback loop. The negative feedback loop is activated in the training process to stabilize training and then removed during inference. The primary challenge lies in how to effectively construct such a feedback loop. Naively utilizing a negatively scaled output of DNN, as in standard negative feedback systems, is not viable because it only leads to a direct scaling of the loss function without modifying the training method.

Instead, we require a negative feedback loop that can track changes in the output while being relatively distinct from it. To meet this requirement, the negative feedback must satisfy two criteria. First, it should be generated by the components that are influenced by the same noise pattern present in the backbone. Second, the negative feedback should have a strong connection with the backbone weights, ensuring that it accurately reflects weight perturbations within the backbone. In NFT, we employ a distinct transformation of the outputs as feedback. Aiming for accurate predictions, the feedback deviating further from the target should have a larger negative impact during training. Let x represent the input data, and the total feedback of a DNN with N feedback outputs is

$$O_{\text{feedback}}(x) = \sum_{n=1}^N \gamma_n \cdot \text{Out}_n \quad (1)$$

where Out_n are feedback outputs generated by NFT and γ_n are decay factors controlling the contribution of each feedback. Combining with backbone output $O_{\text{backbone}}(x) = \text{Output}$ and negative feedback coefficient β , the total output O_{total} is

$$O_{\text{total}}(x) = a_b \cdot O_{\text{backbone}}(x) - a_f \cdot \beta \cdot O_{\text{feedback}}(x) \quad (2)$$

where a_b and a_f are factors influencing the contribution of two outputs. We utilize the widely used Cross-Entropy loss between the total output and the label \hat{y} as our objective

$$\mathcal{L}_{\text{NFT}}(x, \hat{y}) = -\hat{y} \cdot \log(\text{softmax}(O_{\text{total}}(x))) \quad (3)$$

In NFT, during each iteration of the training process, we randomly sample an instance of variation from the Gaussian distribution specific to the target device variations. This sampled variation is then added to the weights in the feed-forward process, and then O_{backbone} and O_{feedback} are generated by NFT. Subsequently, in back-propagation, the objective Eq. 3 is utilized to calculate the gradient in a deterministic manner. Following this, the variation-free weights are updated by the gradient descent algorithm.

There are various methods to generate distinct transformations of the output to form the set of Out_n , and these methods should be adjustable based on specific usage and requirements. In Figure 2, we demonstrate two instances of NFT as reference: Oriented Variational Forward (OVF) in Section 3.2 and Intermediate Representation Snapshot (IRS) in Section 3.3, designed to enhance DNN robustness.

3.2 Oriented Variational Forward

After defining NFT, we introduce a specific implementation, Oriented Variational Forward (OVF), shown in the upper part of Figure 2. OVF generates feedback using the less presentative outputs from oriented variational forwards, which are forward processes with device variations larger than inference variations. Using them as negative feedback, OVF inhibits the backbone’s deviation from the optimal optimization direction. Specifically, in the forward process of the backbone, we sample an instance of variation Δw_i from a Gaussian distribution $\mathcal{D}_{\text{ist}} = \mathcal{N}(0, \sigma^2)$, which is the same as the inference device variations. After applying this noise to backbone weights, the output of the backbone Output is generated. Different from typical training that directly performs back-propagation and weight update afterward, in OVF, we further perform multiple oriented variational forwards based on the same variation-free

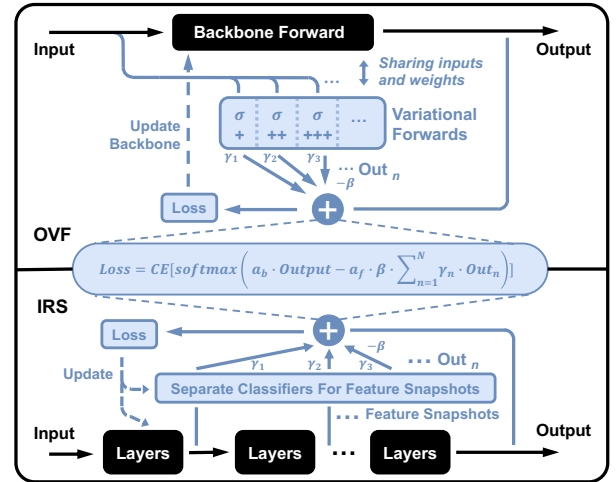


Figure 2: Two example NFT implementations: Oriented Variational Forward (upper) and Intermediate Representation Snapshot (lower).

backbone weight with noises more significant than $\mathcal{N}(0, \sigma^2)$ to collect N negative feedback outputs Out_n . Back-propagation, guided by the NFT objective, initiates only after obtaining all negative feedback. Details are provided in Algorithm 1.

In the selection of hyperparameters, as the standard deviation of the Gaussian distribution increases, noise instances introduce more entropy and uncertainty to the model and its outputs. This results in greater deviations from the target. Consequently, Out_n generated with a larger σ is assigned a larger decay factor γ_n in Eq. 1, providing stronger constraint and negative feedback on the backbone model. We set γ_n as 10^{n-N} to achieve this. These variational forwards generate feedback from the same variation-free backbone weight and use the same Gaussian noise pattern as the backbone variational forward with different parameters, satisfying the criteria outlined in Section 3.1.

3.3 Intermediate Representation Snapshot

In this section, we introduce another specific implementation of NFT, named Intermediate Representation Snapshot (IRS). Concisely, our method utilizes the internal feature representation snapshots as negative feedback in training, illustrated in the lower part of Figure 2. IRS provides the means to observe and regulate the data representations within a neural network during training. In this way, internal perturbations can be reflected in the objective and mitigated through negative feedback.

This method introduces additional transformation components for each feature representation positioned at different depths within a DNN model. Each component operates as an independent probabilistic classifier and transforms the intermediate feature maps to the same shape as the Output of the backbone. The Out_n within the network share portions of the weights and computations present in the backbone.

Choosing the location and number of snapshots in a DNN involves various principles. In this study, we adopt the semantics

Algorithm 1 OVf ($\mathcal{M}, \mathbf{w}, \mathcal{D}ist, ep, \mathbf{D}, \alpha, \beta, N$)

Input: DNN backbone topology \mathcal{M} , weight \mathbf{w} , noise distribution $\mathcal{D}ist$, # of training epochs ep , dataset \mathbf{D} , learning rate α , negative feedback coefficient β , # of negative feedback N ;

```

1: for ( $i = 0; i < ep; i ++$ ) do
2:   for  $x, \hat{y}$  in  $\mathbf{D}$  do
3:     Sample  $\Delta \mathbf{w}_i$  from  $\mathcal{D}ist = \mathcal{N}(0, \sigma^2)$ ;
4:      $\mathcal{O}_{backbone} = \mathcal{M}(\mathbf{w} + \Delta \mathbf{w}_i, x)$ ;
5:     for ( $n = 1; n < N + 1; n ++$ ) do
6:        $\sigma = \sigma + \Delta \sigma$ ;
7:       Sample  $\Delta \mathbf{w}'_n$  from  $\mathcal{N}(0, \sigma^2)$ ;
8:        $Out_n = \mathcal{M}(\mathbf{w} + \Delta \mathbf{w}'_n, x)$ ;
9:        $\mathcal{O}_{feedback} = \sum_{n=1}^N 10^{n-N} Out_n$ ;
10:       $\mathcal{O}_{total} = a_b \cdot \mathcal{O}_{backbone} - a_f \cdot \beta \cdot \mathcal{O}_{feedback}$ ;
11:       $loss(x, \hat{y})$  based on Eq. 3;
12:      Apply update on variation-free weights
13:       $\mathbf{w} := \mathbf{w} - \alpha \frac{\partial loss}{\partial \mathbf{w} + \Delta \mathbf{w}_i}$ ;

```

Output: Robust DNN backbone model $\mathcal{M}(\mathbf{w})$.

principle, treating different types of convolution kernels as distinct functional feature extractors and considering convolution layers with the same kernel depth as one convolution block. Consequently, snapshots are introduced at the end of the respective convolution blocks. Furthermore, to minimize the influence of varying classifier sizes on the results, we configure them with nearly identical layers and parameters.

Algorithm 2 provides the details of the IRS method. By multiplying the outputs from these snapshots with the negative feedback coefficient and utilizing them as a regularizer in the weight update, we can effectively enhance the system’s robustness against “external noise”.

The representations closer to the output of the backbone capture more intricate feature information and deviate less from the target output. As a result, they are assigned a smaller decay factor. Specifically, in Eq. 1, $\gamma_n = 10^{1-n}$ for each feedback output Out_n . This approach ensures that the feedback’s impact is reduced as the snapshots handle more complex features. To ensure that the snapshots accurately represent noise and data flow, we introduce noise to the classifiers, similar to the approach used in the backbone, and simultaneously update the weights of both the backbone and classifiers.

4 EXPERIMENTS

4.1 Model Weight Perturbation

Without loss of generality, we primarily consider device variations stemming from the programming process, where the programmed conductance value in NVM devices deviates from the desired value. We will then demonstrate how to model the influence of these device variations on DNN weights.

Let a DNN weight be M bits, the desired weight value \mathcal{W}_d after quantization is

$$\mathcal{W}_d = \frac{\max |\mathcal{W}|}{2^M - 1} \sum_{i=0}^{M-1} m_i \times 2^i \quad (4)$$

Algorithm 2 IRS ($\mathcal{M}, \mathcal{C}, \mathbf{w}, \mathcal{D}ist, ep, \mathbf{D}, \alpha, \beta, N$)

Input: DNN backbone topology \mathcal{M} , Classifiers topology \mathcal{C} , weight \mathbf{w} , noise distribution $\mathcal{D}ist$, # of training epochs ep , dataset \mathbf{D} , learning rate α , negative feedback coefficient β , # of negative feedback N ;

```

1: for ( $i = 0; i < ep; i ++$ ) do
2:   for  $x, \hat{y}$  in  $\mathbf{D}$  do
3:     Sample  $\Delta \mathbf{w}_i$  from  $\mathcal{D}ist = \mathcal{N}(0, \sigma^2)$ ;
4:     Collect  $Output$  and  $Out_n$  synchronously with
5:      $\mathcal{M}(\mathbf{w} + \Delta \mathbf{w}_i, x)$  and  $\mathcal{C}(\mathbf{w} + \Delta \mathbf{w}_i, x)$ ;
6:      $\mathcal{O}_{feedback} = \sum_{n=1}^N 10^{1-n} Out_n$ ;
7:      $\mathcal{O}_{total} = a_b \cdot \mathcal{O}_{backbone} - a_f \cdot \beta \cdot \mathcal{O}_{feedback}$ ;
8:      $loss(x, \hat{y})$  based on Eq. 3;
9:     Apply update on variation-free weights in  $\mathcal{M}, \mathcal{C}$ 
10:     $\mathbf{w} := \mathbf{w} - \alpha \frac{\partial loss}{\partial \mathbf{w} + \Delta \mathbf{w}_i}$ ;

```

Output: Robust DNN backbone model $\mathcal{M}(\mathbf{w})$.

where \mathcal{W} represents floating-point weights and $\max |\mathcal{W}|$ denotes the maximum absolute value among weights, and $m_i \in \{0, 1\}$ signifies the value of i^{th} bit of the desired weight value. For a NVM device representing K bits data, each weight can be stored in M/K devices¹ and the mapping process is $\bar{g}_j = \sum_{i=0}^{K-1} m_{j \times K + i} \times 2^i$ where \bar{g}_j is the desired conductance of the j^{th} device. Note that negative weights can be mapped in the same manner to a separate crossbar array. Considering the device variation, the actual device conductance after programming is denoted as $g_j = \bar{g}_j + \Delta g$, where Δg represents the deviation from the desired conductance value \bar{g}_j and follows a Gaussian distribution. So the actual weight \mathcal{W}_p represented by programmed NVM devices is

$$\mathcal{W}_p = \mathcal{W}_d + \frac{\max |\mathcal{W}|}{2^M - 1} \sum_{j=0}^{M/K-1} \Delta g \times 2^{j \times K} \quad (5)$$

We used parameter settings based on previous works [9, 16, 20]. Specifically, we set $K = 2$, while the value of M depended on the specific model configuration. In this study, we choose $M = 8$, indicating 8-bit precision for a single DNN weight and 2-bit precision for a single device conductance. For device variation, we adopt a Gaussian distribution with $\Delta g \sim \mathcal{N}(0, \sigma_d^2)$, where the σ_d represents the relative standard deviation of conductance corresponding to the maximal conductance of a single device. We impose the constraint $\sigma_d \leq 0.4$ as this falls within a reasonable range achievable through device-level optimizations, such as write-verify based on measurement results. Our model and parameter settings align with those of RRAM devices described in [16].

To evaluate the performance of our proposed method on the NVCIM DNN accelerator, we conducted a Monte Carlo simulation using noise-injection inference. In each inference simulation run, noise was independently sampled from the same Gaussian distribution. We calculated the average accuracy across these simulation runs. As shown in Figure 1(b), only the backbone weight of the model is utilized during the inference process.

¹For simplicity, we consider M to be a multiple of K .

4.2 Experimental Setup

We conducted experiments using the PyTorch environment on NVIDIA GPU. Unless otherwise specified, reported results represent the average of at least five independent runs. We employed the average accuracy of noise-injection inference as the performance metric and conducted a Monte Carlo simulation with 200 runs for sufficiently high precision. Our experiments reveal that the results have a 95% confidence interval of ± 0.01 , in accordance with the central limit theorem.

We compare NFT with two baselines: 1) vanilla training (W/O Noise) and 2) Gaussian noise-injection training (W/ Noise) [9, 21]. We did not assess NFT against other orthogonal methods like NAS-based DNN topology design or Bayesian Neural Networks, as NFT can be used in conjunction with them.

In our experiments with extensive datasets and neural network backbones, we find that the optimal value of negative feedback coefficient β can always be found in the following set $\{1e-1, 1e-2, 1e-3, 1e-4\}$. As such, a four-step search is sufficient to find the optimal setting.

For hyperparameter values, we set $start = 0$ and $end = 2 \times \sigma_d$ and evaluate the effectiveness of NFT across different σ_d values within the range mentioned in Section 4.1, and set contribution factors $a_b = a_f = 1/(N+1)$, where N is the number of negative feedback. Other training hyperparameters, such as learning rate, batch size, and learning rate schedulers, follow best practices for training a noise-free model.

4.3 Effectiveness of Accuracy Improvement

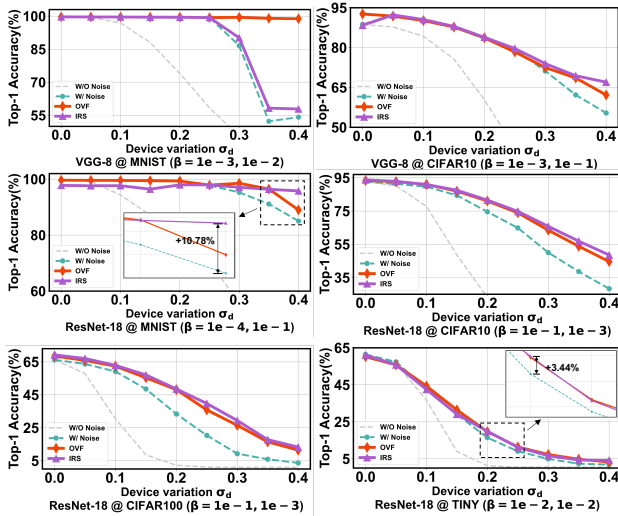


Figure 3: Effectiveness of NFT, implemented by proposed instances (OVF and IRS): Average noisy inference accuracy on VGG-8 and ResNet-18 backbone models for different datasets across σ_d values. The negative feedback coefficients β are for OVF and IRS.

For experiments, we use the VGG-8 [14] backbone on MNIST and CIFAR10 datasets, and the ResNet-18 [8] backbone on MNIST, CIFAR10, CIFAR100, and Tiny ImageNet datasets.

In OVF, we empirically set negative feedback $N = 3$ for VGG-8 and ResNet-18, with each increase $\Delta\sigma_d$ fixed at 0.05. The VGG-8 model consists of 6 convolutional layers with 4 types of semantic convolution kernels, while the ResNet-18 model has 17 convolutional layers with 5 types of semantic convolution kernels. So, in IRS, negative feedback is set to $N = 3$ for VGG-8 and $N = 4$ for ResNet-18, guided by the semantics principle presented in Section 3.3. For clarity, the classifiers in IRS are composed of an average pooling layer followed by two fully connected layers. In addition, the negative feedback coefficient β for each model on a specific dataset is determined through a four-step search, as discussed in Section 4.2.

Figure 3 shows the Top-1 accuracy of models with different training methods under different levels of device variations σ_d following the noise model discussed in Section 4.1. Both OVF and IRS clearly outperform all baselines in most device value deviation values and perform similarly as baselines in some rare cases where device value deviation is too small to make an impact. Compared with Gaussian noise-injection training baseline, OVF improves the Top-1 accuracy by up to 46.71%, 6.78%, 5.35%, 16.30%, 17.21%, and 3.22%, while IRS improves by up to 5.98%, 11.60%, 10.78%, 20.24%, 20.10%, and 3.44% in VGG-8 for MNIST and CIFAR-10, ResNet-18 for MNIST, CIFAR-10, CIFAR-100, and Tiny ImageNet, respectively. OVF constrains the network based on the overall forward performance and is more suitable for smaller networks that have not reached the limit of their representation ability, like VGG-8 on MNIST. On the other hand, IRS performs slightly better in deeper networks with internal representation constraints, such as ResNet-18 on CIFAR-10.

The effectiveness of the two instances of NFT: OVF and IRS underscores the generality and practicality of NFT in enhancing DNN robustness against device variation.

4.4 Uncertainty and Convergence

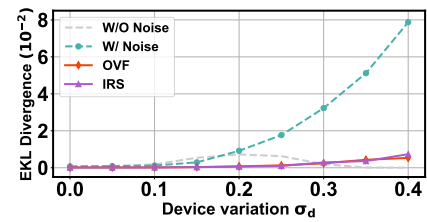


Figure 4: Average EKL divergence for correct predictions with different methods.

Device variation amplifies epistemic uncertainty, leading to increased output uncertainty. We utilize Expected Kullback–Leibler (EKL) Divergence [7] (the lower the better) to quantify the impact of device variation on uncertainty. To ensure a fair comparison, accuracy is excluded from the analysis. Specifically, among all correct predictions in noisy inference, we calculate the Kullback–Leibler Divergence between each softmax output and its corresponding label. The results are the average EKL divergence for each correct prediction, shown in Figure 4. Compared to the W/O Noise baseline, W/ Noise baseline enhances accuracy but at the cost of increased uncertainty. In contrast, our NFT not only achieves even higher accuracy than the noise-injection training baseline but also maintains

low uncertainty and high confidence in the output. In cases where device variation is too substantial for effective predictions using the vanilla training baseline, its EKL divergence appears slightly lower than that of NFT, as it generates completely random and meaningless predictions.

For certain devices and aging-related issues, the device variation can be large. The low uncertainty achieved by NFT also contributes to model convergence. For instance, in 10 separate runs of experiments with VGG-8 on MNIST using $\sigma_d = 0.35$, the number of non-converging models² is 6, 0, and 2 for noise-injection training, OVF, and IRS, respectively. Besides the increase in accuracy, this may also partially explain the substantial improvement of OVF in VGG-8 for MNIST, as shown in Figure 3.

4.5 Ablation Study

In this section, we present ablation studies for NFT. The example experiments use ResNet-18 on the CIFAR-10 dataset, incorporating device variation with $\sigma_d = 0.3$.

Different N of negative feedback: Table 1 shows the noisy inference accuracy when we try to use different numbers of negative feedback Out_n in NFT. It shows that our setting achieves the best accuracy, which is $N = 3$ for OVF and $N = 4$ for IRS. Although continuing to increase the number of negative feedback tends to result in a slight improvement in accuracy, we maintained the current settings (marked as *) due to considerations of time and energy efficiency.

Table 1: The impact of the # of negative feedback Out_n .

Negative Feedback Out_n	1	1+2	1~3	1~4	1~5
OVF Acc.(%)	57.24	61.60	63.50*	65.67	-
IRS Acc.(%)	55.93	61.58	65.43	65.81*	66.44

Reverse Decay Factors: In this scenario, we reverse the direction of decay factors γ_n . Specifically, for feedback demonstrating a greater deviation from the target, we assign a smaller γ_n . This configuration stands in contrast to that utilized in NFT. With the reversed decay factors, OVF and IRS exhibit 46.01% and 44.90% inference accuracy, respectively, compared to 63.50% and 65.81% in NFT experiments. This reduction reinforces our initial configuration and emphasizes the unique roles played by each negative feedback in NFT. Feedback with a greater deviation should exert a larger influence on the training process, thereby constraining the backbone network toward the optimal point.

Reverse Oriented σ_d : In this experiment, we focus on OVF as our goal is to use less representative forward outputs as feedback to constrain the backbone’s deviation from the optimal optimization direction. Here we enable oriented variational forwards to generate improved outputs by adjusting $\Delta\sigma_d$ from +0.05 to -0.05. The results demonstrate a 14.14% drop in accuracy, supporting our original claims.

²where accuracy decreases by more than 5% compared to the average accuracy across multiple independent runs

Noise in Classifiers: In Section 3.3, we also introduce noise into each classifier’s weight to ensure that the impact of device variation within the backbone is completely presented to the objective by representation snapshots, aiding backbone training through NFT. In subsequent experiments, we removed the noise in classifiers during training, resulting in an accuracy of 48.44%, lower than the 65.81% achieved in NFT experiments.

Pretrained Models: To assess whether training time and energy can be saved by pretrained models, we use a pretrained model trained through the vanilla training method for 200 epochs (accuracy 92.71% with $\sigma_d = 0$) in NFT. The noisy inference results are presented in Table 2. The findings indicate that the optimal approach for NFT is training from scratch, as implemented in our previous experiments (marked as *).

Table 2: Applying NFT with and without pretrained models.

Models	Pre +0 ep	Pre +50 ep	Pre +100 ep	Pre +200 ep	From Scr. 200 ep
OVF Acc.(%)	10.75	55.97	57.15	56.05	63.50*
IRS Acc.(%)	10.75	55.07	57.34	56.94	65.81*

5 CONCLUSION

In this study, we introduce a novel concept—**Negative Feedback Training (NFT)**—to improve the robustness of the DNN accelerators and propose two instances to implement this NFT concept, namely *oriented variational forward (OVF)* and *intermediate representation snapshot (IRS)*. Both OVF and IRS showcase the capability to enhance the robustness of DNN models, underscoring the generality and practicality of NFT. Experimental results, conducted across various neural architectures and datasets, reveal that our proposed method achieves significant improvements over state-of-the-art baselines in terms of enhancing the robustness of the DNN models and reducing the uncertainty caused by device variations.

REFERENCES

- [1] Chen et al. 2009. Highly scalable hafnium oxide memory with improvements of resistive distribution and read disturb immunity. In *IEDM*.
- [2] Chen et al. 2016. Eyeriss: A spatial architecture for energy-efficient dataflow for convolutional neural networks. *ACM SIGARCH* (2016).
- [3] Degraeve et al. 2015. Causes and consequences of the stochastic aspect of filamentary RRAM. *Microelectron. Eng.* (2015).
- [4] Eldebiky et al. 2023. CorrectNet: Robustness Enhancement of Analog In-Memory Computing for Neural Networks by Error Suppression and Compensation. In *DATE*.
- [5] Feinberg et al. 2018. Making memristive neural network accelerators reliable. In *HPCA*.
- [6] Gao et al. 2021. Bayesian inference based robust computing on memristor crossbar. In *DAC*.
- [7] Gawlikowski et al. 2023. A survey of uncertainty in deep neural networks. *AI Rev.* (2023).
- [8] He et al. 2016. Deep residual learning for image recognition. In *CVPR*.
- [9] Jiang et al. 2020. Device-circuit-architecture co-exploration for computing-in-memory neural accelerators. *IEEE Trans. Comput.* (2020).
- [10] Jin et al. 2020. On improving fault tolerance of memristor crossbar based neural network designs by target sparsifying. In *DATE*.
- [11] Qin et al. 2020. Design of high robustness BNN inference accelerator based on binary memristors. *IEEE Trans. Electron Devices.* (2020).
- [12] Rizzi et al. 2011. Role of mechanical stress in the resistance drift of Ge₂Sb₂Te₅ films and phase change memories. *Appl. Phys. Lett.* (2011).
- [13] Raty et al. 2015. Aging mechanisms in amorphous phase-change materials. *Nat. Commun.* (2015).

- [14] Simonyan et al. 2014. Very deep convolutional networks for large-scale image recognition. *arXiv:1409.1556* (2014).
- [15] Shafiee et al. 2016. ISAAC: A convolutional neural network accelerator with in-situ analog arithmetic in crossbars. *ACM SIGARCH* (2016).
- [16] Shim et al. 2020. Two-step write-verify scheme and impact of the read noise in multilevel RRAM-based inference engine. *Semicond. Sci. Technol.* (2020).
- [17] Wan et al. 2022. Accuracy and resiliency of analog compute-in-memory inference engines. *JETC* (2022).
- [18] Yan et al. 2021. Uncertainty Modeling of Emerging Device based Computing-in-Memory Neural Accelerators with Application to Neural Architecture Search. In *ASP-DAC*.
- [19] Yan et al. 2022. Computing-In-Memory Neural Network Accelerators for Safety-Critical Systems: Can Small Device Variations Be Disastrous?. In *ICCAD*.
- [20] Yan et al. 2022. SWIM: Selective Write-Verify for Computing-in-Memory Neural Accelerators. In *DAC*.
- [21] Yang et al. 2022. Tolerating Noise Effects in Processing-in-Memory Systems for Neural Networks: A Hardware-Software Codesign Perspective. *Adv. Intell. Syst.* (2022).
- [22] Zhang et al. 2023. Edge learning using a fully integrated neuro-inspired memristor chip. *Science* (2023).